Optimization of irradiance for photodynamic therapy of port-wine stain

Feng-juan Zhang
Xiao-ming Hu
Ya Zhou
Qin Li

Optimization of irradiance for photodynamic therapy of port-wine stain

Feng-juan Zhang,[a] Xiao-ming Hu,[a,*] Ya Zhou,[b] and Qin Li[a]
[a]Beijing Institute of Technology, School of Life Science, Beijing 100081, China
[b]Beijing Institute of Technology, School of Optoelectronics, Beijing 100081, China

Abstract. Controllable and effective irradiation of lesions is among the key factors that affect the potency of photodynamic therapy (PDT). An optimization method for the irradiance distribution of treatment was proposed which can be used to improve the efficacy of PDT and allow more lesions to receive the desired irradiance level in a single therapy session. With the proposed digital illumination binocular treatment system, the preferred surface normal vectors, irradiation angles, as well as area and weight coefficients of lesions can be achieved and used as characteristic parameters to optimize the irradiation direction. Two port-wine stain phantom experiments were performed. The comparison of the illumination area between preoptimization and postoptimization showed that the proposed method can effectively guide the light source control, improve the distribution of light dose, and increase the effective treatment area. © *2015 Society of Photo-Optical Instrumentation Engineers (SPIE)* [DOI: 10.1117/1.JBO.20.4 .048004]

1 Introduction

Port-wine stain (PWS) is a congenital disease caused by hyperplasia and dilatation of skin capillaries.[1–3] Pathological changes caused by PWS commonly occur in face and neck, where lesions gradually become darker and thicker as the patient ages. PWS affects ∼25 million people worldwide, and its lesions will not regress without medical intervention.[4,5] This disease not only affects the appearance of an individual, but also his/her psychological and physical health.

Many therapeutic methods (surgical excision, cryosurgery, and dermabrasion) can be used to treat PWS, but they are outmoded because of their ineffectiveness and adverse secondary effects (e.g., scarring). The use of a pulsed dye laser (PDL) with wavelengths of 585 or 595 nm is the current gold standard for PWS treatment,[6–8] but only a few lesions are completely lightened in this method. Approximately 20 to 30% of patients who underwent PDL are considered "poor responders," and up to 20% of the lesions are not lightened.[9]

Clinical studies suggested that photodynamic therapy (PDT) is a promising alternative treatment for PDL-resistant PWS lesions.[10,11] The General Hospital of the People's Liberation Army in China uses PDT to treat PWS. This treatment presented more significant improvements in the long-term outcomes with no recurrence. Another clinical study retrospectively reviewed 642 Chinese patients who received PDT therapy (a total of 3066 treatment sessions) within a five-year period from March 2004 to February 2009; 70% of the patients exhibited >25% clearing, >29.8% presented clearing of >50%, and the patient satisfaction score increased to 7.8.[12] In 2014, a long-term follow-up (after 18 years) showed that PDT provided stable results in treating PWS and the lesions did not recur after their complete removal.[13] The safety and efficiency of PDT

were proven by several clinical tests;[14–16] nevertheless, large-scale prospective, comparative, and controlled clinical studies must be conducted to elucidate the complex relationship between treatment outcomes and light parameters, as well as standardize PDT procedures.

Complete clearance of severe lesions remains poor despite multiple PDT treatments as indicated in several clinical trials. Gu et al.[17] reported a total clearance of only 128 (6.6%) among 1942 lesions in 1385 patients. Xiao et al.[12] also revealed that ∼5% of the patients exhibited complete clearance. As inferred from these studies, the outcomes of PDT for the treatment of PWS remain restricted by inadequate information on lesions[11] and unavailable optimal control systems.

Light is among the primary factors that affect the efficacy of PDT,[18,19] which is strongly influenced by the wavelength and the treatment dosage. Light sources with wavelengths of 532, 510, and 578 nm are currently used in PDT for treatment of PWS; similarly, 457 nm may be potentially applied in PDT for treatment of pink or flat red PWS among infants.[20] Treatment dosage is proportional to the irradiance of light sources, illumination time, and the cosine value of the irradiation angle; by contrast, the dosage is inversely proportional to the square of the irradiation distance from a plane light source. The effectiveness of the treatment is constrained by personal experience because light devices are usually controlled through manual operation; hence, comparison and optimization are difficult, particularly in cases with Gauss-shaped irradiance distribution of the laser source. In current research and clinical therapy,[20] the common light irradiances used for adults and infants are 100 and 80 mW/cm^2, respectively, which are simply achieved by dividing the total power by the illumination area; nevertheless, determining the actual irradiance on the lesions remains

a challenge because of their curved shape. Moreover, a local light dose that is higher or lower than the required dosage will induce inconsistent changes in blood flow, oxygen concentration, photosensitizer consumption within local areas, and various degrees of pain; these changes may increase the risks of adverse effects or ineffective treatment.[21] Additional parameters must be established to accurately control illumination and develop individualized single treatment plans, thus reducing the incidence of adverse effects and improving the efficacy of PDT for treatment of PWS.[21–25]

Precise control of the light dose is dependent on the performance of a control system rather than subjective experiences and assessments. So an intelligent irradiation system with a large coverage and flexible conformity should be designed to increase the reliability and consistency of PDT. Zhu et al.[22] evaluated the laser source position and patient contour by using an infrared navigation system to calculate a real-time light dose.[22] In their investigation, the light dose was monitored using seven detectors to guide light source motion and achieve a uniform light dose distribution. Wang et al.[23] solved the spatial relationship between the locations of light sources and lesions by introducing a robotic system, in which the irradiation position and movement speed of the laser source are controlled by simulating hand movements to ensure a uniform distribution of light.[23]

In this research, an optimization method is proposed to determine the optimal irradiation direction and establish a digital treatment system, which can record, evaluate, and compare treatment dosages and must be effective in one treatment session. First, the point cloud of lesions was reconstructed and preprocessed and their feature parameters were determined. Second, an iterative optimization method with weight coefficients was presented. Finally, two phantom experiments were conducted to verify the feasibility and validity of the proposed method.

2 Materials and Methods

2.1 System Configuration and Optimization Roadmap

A treatment system consisting of a binocular vision system and an image progress unit was used for three-dimensional (3-D)

reconstruction of lesion areas; this reconstructed model will serve as the objective basis to optimize the direction of the irradiation treatment.[24,25] As shown in Fig. 1(a), the proposed model for binocular digital illumination comprised a camera, digital projector, and computing unit. A camera (Nikon D3200, Tokyo, Japan) with 3008×2000 pixels was used to capture images during the process. A projector (Sony VPL-DX120, KōnanMinato, Tokyo, Japan) with 1024×768 pixels was applied as a space modulator in 3-D reconstruction and as a light device in the treatment. In the experiment, two head models painted with red color were used to represent the patient with PWS lesions.

The majority of lesions should receive the required irradiance dosage during treatment. The distribution of light irradiance was optimized by dividing the lesions into small patches and mapping them to the corresponding pixels on the projector. This map was used to control the irradiance on the lesion by adjusting the gray value of the video signals to the projector.

The software for optimization included preprocessing of the point cloud of lesions, calculating the irradiance angle, incorporating weight coefficients in the optimization function, and evaluating irradiation [Fig. 1(b)]. The flow path is introduced in detail in the following sections.

2.2 Parameters for Optimization

After the camera-projector vision system was calibrated, 3-D modeling of the head was conducted through a gray-coded structured light method based on ray-plane triangulation. The pixels in the camera image and the 3-D points share one-to-one mapping. Digital color images of the skin were used to segment the lesions, and 3-D lesion coordinates were indexed from the two-dimensional projector image.[24,25] Although previous studies specified that the point clouds obtained using structured light measurements with MeshLab exhibited high reconstructive accuracy,[24] error points may still exist because of incorrect lesion extraction. Processing the point clouds and calculating the characteristic parameters of the lesion surface are important in optimization to accurately characterize the surface features of lesions.

a:The projector   c:The lesions
b:The camera   d:The normal skin

(a)

(b)
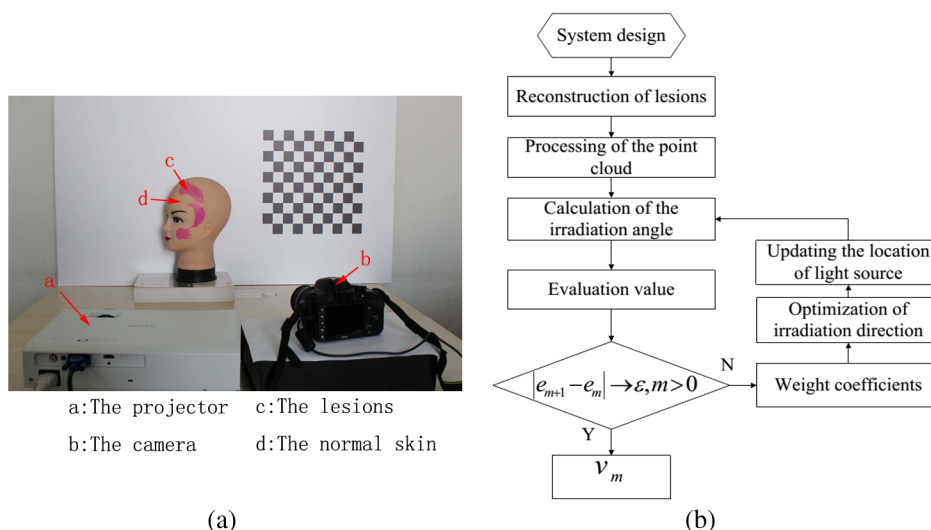
Fig. 1 (a) System setup and (b) flow chart of optimization.

2.2.1 Preprocessing of point clouds

Moving least squares (MLS) was used as a mesh-free method for effective smoothing, error point removal, and approximation and interpolation of the point cloud of lesions.[26–29] The moving region around the test point $p(x, y, z)$ in the 3-D space was determined using the search radius. Supposing that k points were located in the moving region and $k < 3$, the point $p(x, y, z)$ was considered the error point and was removed from the point cloud of lesions. The moving region with points more than three was marked as the region of interest in which smoothing was performed.

In MLS, the local function in the moving region of interest with k points around p is defined in terms of function $B(p)$ and several $\alpha(p)$ coefficients[26,27] as shown in Eq. (1):

$$f(p) = B^T(p)\alpha(p), \tag{1}$$

where $B(p)$ refers to the selected complete polynomial bases, and the linear bases are expressed as $B(p) = [1 \quad x \quad y \quad z]^T$. $\alpha(p)$ coefficients are determined using a weighted least squares method, which minimizes the objective function $J(\alpha)$. $J(\alpha)$ is then expressed as

$$J(\alpha) = \sum_{i=1}^{k} w(\|p_i - p\|)[f(p) - f(p_i)]^2, \tag{2}$$

where the weighting function $w(\|p_i - p\|)$ is defined to ensure $w > 0$ as

$$w(d_i) = \frac{e^{-\frac{d_i^2}{h^2}}}{d_i^2}, \tag{3}$$

where $d_i = \|p_i - p\|$ and h is the spacing parameter. A low h value may cause the function to decay faster and the approximation to be more local; the assigned weight $1/d_i^2$ is used to control the influence of the local feature on the approximation, which forces the MLS fitting function to interpolate the prescribed function values in these points within the moving region and avoid outliers.[29–31]

2.2.2 Normal vectors

Irradiance is proportional to the cosine value of the irradiation angle, which is defined as the angle between the normal and illumination direction vectors. The normal vectors of the lesion surface were calculated to characterize their features. The surface normal of each patch was measured using a conventional method. Normal vectors were calculated using a classical k-nearest neighbor algorithm in the moving region in MLS. The k points surrounding the point p were listed as an array $\{p_1, p_2, \ldots, p_k\}$. In addition, the 3×3 covariance matrix C for the sample point p can be obtained using the following equation:

$$C = \sum_{i=1}^{k} (p_i - \bar{p}) \cdot (p_i - \bar{p})^T, \tag{4}$$

where $\bar{p}$ is the center of the k neighborhood points.

Consider the eigenvector equation

$$C \cdot \vec{v}_j = \lambda_j \cdot \vec{v}_j, \qquad j \in \{1,2,3\}, \tag{5}$$

where λ_j is the eigenvalue and $\vec{v}_j$ is the eigenvector. Assuming $\lambda_0 \leq \lambda_1 \leq \lambda_2$, the plane $T(p')$ through $\bar{p}$ minimizes the sum of the squared distances to the neighbors of p.

$$T(p'): (p' - \bar{p}) \cdot \vec{v}_0 = 0. \tag{6}$$

The eigenvector that corresponds to the minimum eigenvalue can be considered as the normal vector of the point p.[32]

2.2.3 Triangularization of lesions

The Delaunay method was applied to triangulate the point cloud of lesions and acquire the statistic of the illumination area. The area of each triangle patch was individually calculated and totaled to approximate the area of lesions. When the projector was used as the treatment light source, the corresponding pixel P_p in the projector image that matched the parameters of the binocular system was used to control irradiation.

The difference in the irradiance received by the small triangle patches can be identified based on the irradiation angle. In the method described in Sec. 2.2.2, the normal vector for each point in the lesions can be calculated. The surface normal vector of the triangle patch was also set according to the fitting of the corresponding normal vectors of the triangle's vertices.

As shown in Fig. 2, the irradiation angle θ is the angle between the incident ray O_pP and the surface normal $\vec{n}$ of the patch. $O_p - X_p Y_p Z_p$ represents the coordinates of the projector, and P_p is the control pixel in the projector image for the irradiance of the patch. The cosine of θ is defined in Eq. (7):

$$\cos \theta = \frac{\vec{PP_p} \times \vec{n}}{|\vec{PP_p}||\vec{n}|}. \tag{7}$$
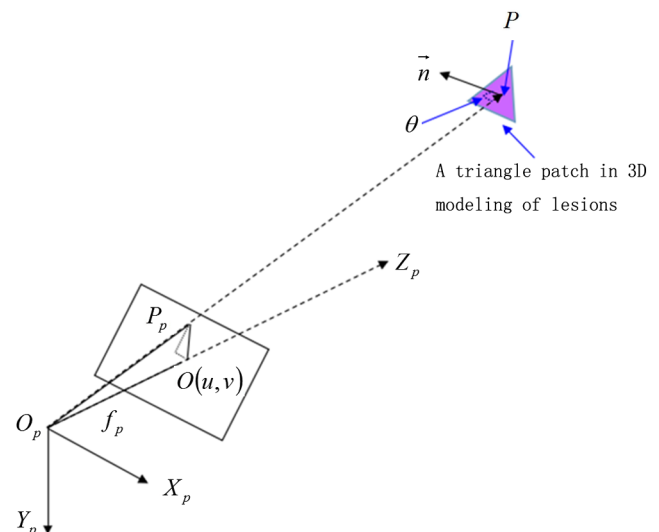
Fig. 2 Irradiation angle of a patch.

2.3 Optimization

An iterative optimization method with weight coefficients is proposed to optimize the irradiation and achieve the maximum lesion area in a single session. The weight coefficients were established according to the distribution area of irradiation. The optimization function was defined in terms of the weight coefficients and normal vectors of the lesions. The location of the light source was updated based on the optimized vector.

2.3.1 Evaluating irradiation

When the light source treated the lesions in a specific direction, the merit value in Eq. (8) was used to evaluate the irradiance received by the lesions; this value is the sum of the product of the cosine values of the irradiation angles and the area of each triangle patch. Given that irradiance is proportional to the cosine value, this research posited that more light energy can be utilized during treatment with a higher irradiation value. Hence,

$$e = \sum_{i=1}^{N} s_i \cos \theta_i, \qquad (8)$$

where θ_i is the irradiation angle of the i'th patch, s_i is the area of the patch, and N is the number of triangle patches. During optimization, the assessed value of the initial irradiation is set as e_0. This value can characterize the optimization results to determine the optimal irradiation direction.

2.3.2 Determination of optimization function

The proposed method aimed to expand the area that receives adequate irradiance in a single therapy session when the power of the light source is constant. As discussed in Sec. 2.2.3, the illumination area with different irradiances can be divided according to the cosine value of the irradiation angle. Therefore, the triangle patches were classified by dividing the cosine scope into k intervals. Area statistics were established in the same cosine interval to estimate the distribution of the illumination area with different irradiances. The areas of the regions with high cosine values may be increased by selecting the optimal irradiation direction. Thus, the weight coefficients were incorporated in the optimization function according to the percentage of the area. The weight coefficient is defined as

$$w_j = \frac{\Delta S_j}{S}, \qquad j \in [1, k], \qquad (9)$$

where S is the total area of the lesions and ΔS_j is the area of the triangle patches with cosine values in the j'th interval.

The irradiation direction vector was optimized with weight coefficients on the basis of the normal directions of the triangle patches, as shown in Eq. (10):

$$v = \sum_{j=1}^{k} w_j \Delta n_j, \qquad (10)$$

where Δn_j is the fitted vector based on the normal directions of the triangle patches. The unit vector v is the updated irradiation direction vector.

2.3.3 Updating the position of the light source

The projector was located at a specific distance from the patient. Suppose the point set of lesions is

$$\Omega = \{p_1(x_1, y_1, z_1), p_2(x_2, y_2, z_2), \ldots, p_n(x_n, y_n, z_n)\}.$$

At the beginning of optimization, the projector was translated to enable its optic axis to pass through the initial point for the direction optimization $G(x_0, y_0, z_0)$ with

$$\begin{cases} x_0 = \frac{x_{\min} + x_{\max}}{2} \\ y_0 = \frac{y_{\min} + y_{\max}}{2}, \\ z_0 = \frac{z_{\min} + z_{\max}}{2} \end{cases} \qquad (11)$$

where

$$\begin{cases} x_{\min} = \min(x_1, x_2, \ldots, x_n), x_{\max} = \max(x_1, x_2, \ldots, x_n) \\ y_{\min} = \min(y_1, y_2, \ldots, y_n), y_{\max} = \max(y_1, y_2, \ldots, y_n). \\ z_{\min} = \min(z_1, z_2, \ldots, z_n), z_{\max} = \min(z_1, z_2, \ldots, z_n) \end{cases} \qquad (12)$$

In optimization, the optic axis of the projector passed through the initial point. In iteration, the position of the light source was updated according to the optimization results to irradiate the lesions in a new irradiation direction as shown in Fig. 3. $O_p - X_p Y_p Z_p$ and $O_p' - X_p' Y_p' Z_p'$ represent the original and updated positions of the projector, respectively. $O(u, v)$ is the optical center of the projector, and f_p is the focal length of the projector that remains constant to avoid recalibration and reduce complexity. The distance between G and the optical axis is L, and $\vec{v}$ is the optimized vector. The irradiation angles are θ and θ' when the projector irradiated the lesions at the original and updated positions, respectively. The updated position $O_p'(X, Y, Z)$ can be calculated using Eq. (13):

$$\begin{bmatrix} X \\ Y \\ Z \end{bmatrix} = \begin{bmatrix} x_0 \\ y_0 \\ z_0 \end{bmatrix} + \beta\vec{v}, \qquad (13)$$

where $\sqrt{(\beta\vec{v})(\beta\vec{v})^T} = L + f_p$.
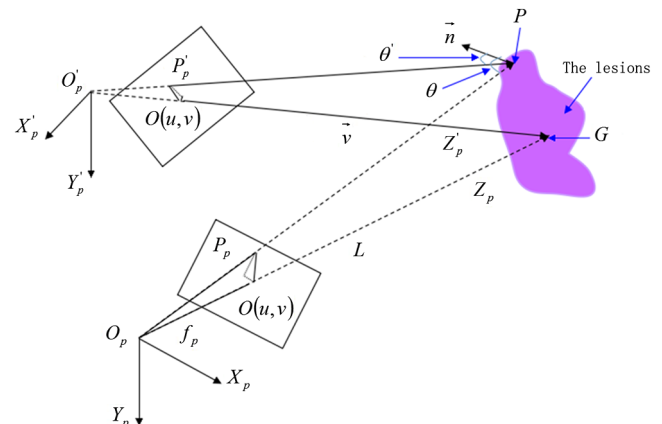
Fig. 3 Three-dimensional diagram of the updated position.
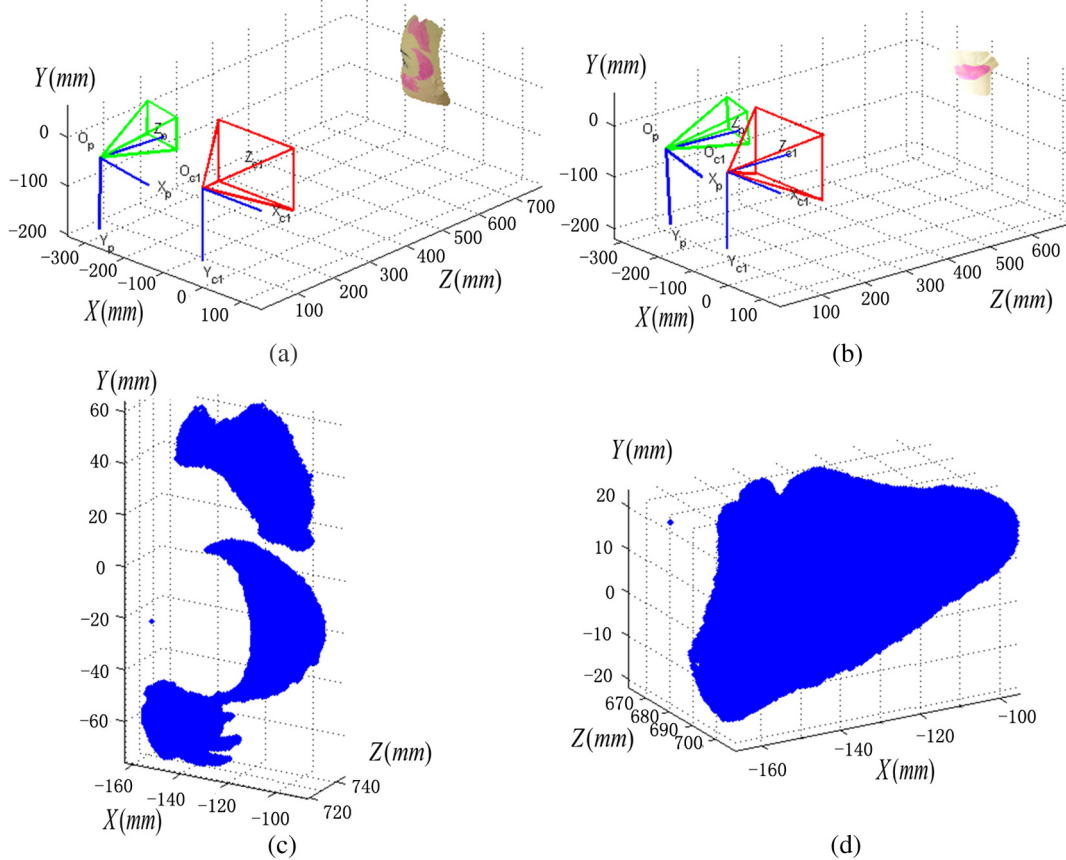
Fig. 4 Reconstruction of lesions in the two experiments: region of interest reconstruction in experiments (a) I and (b) II, and the point cloud of lesions in experiments (c) I and (d) II.

3 Results

3.1 Reconstruction of Lesions

PWS lesions were represented by the two head models painted on the face and neck, where PWS frequently occurs. The regions of interest in the head models are shown in Figs. 4(a) and 4(b). The point clouds of lesions were also extracted and shown in Figs. 4(c) and 4(d).

3.2 Processing Point Clouds

The point clouds processed with filtering and smoothing are shown in Fig. 5. In smoothing, the order of the basis function was 4 and the Gaussian function was used as the weighting function. Comparison of the processed and original data in experiments I [Figs. 4(c) and 5(a)] and II [Figs. 4(d) and 5(b)] revealed that the error points were removed. The smoothing degrees of the model data were also significantly improved.

The point clouds were triangulated as discussed in Sec. 2.2 and shown in Figs. 5(c) and 5(d). The numbers of triangles in the two experimental lesions were 69,756 and 44,442, with total lesion areas of 105.7 and 42.5 cm^2, respectively. The area, normal vector, and location of the center of gravity of each triangle were stored and used as basic parameters for optimizing the irradiation direction.

3.3 Optimizing Irradiation Direction

In each iterative process, the cosine value of the irradiation angle of each triangle irradiated in the previous direction was calculated. This value may be negative because the curvature radii varied in different patches of the complex curved lesion surface. The cosine values were then divided into 11 intervals, and data with non-negative numbers were classified into one interval.

The optimized vector was calculated using Eqs. (9) and (10), and the irradiation angle for each patch irradiated in the optimized direction was determined. The sum of the products of the cosine values and area were calculated to assess irradiation and reveal the optimization result. When e is closer to the area of the lesions, the optimization is more effective and the lesions can receive more irradiance. The values of e during the five iterations in experiments I and II are shown in Fig. 6.

Statistical analysis of e indicated that the optimization result can achieve a steady state after five iterations despite the occurrence of a slight fluctuation. The value of e_0 was evaluated at the original irradiation, and the second e value of e_1 was calculated by adjusting the optical axis of the projector to pass through the initial point and thus optimize the original irradiation direction. Although this value may be lower than e_0 as shown in Fig. 6(b), it can also reach its best value in the following optimization steps. The optimized vectors in the fifth and fourth optimization represented the optimal irradiation direction vectors for experiments I and II, respectively.
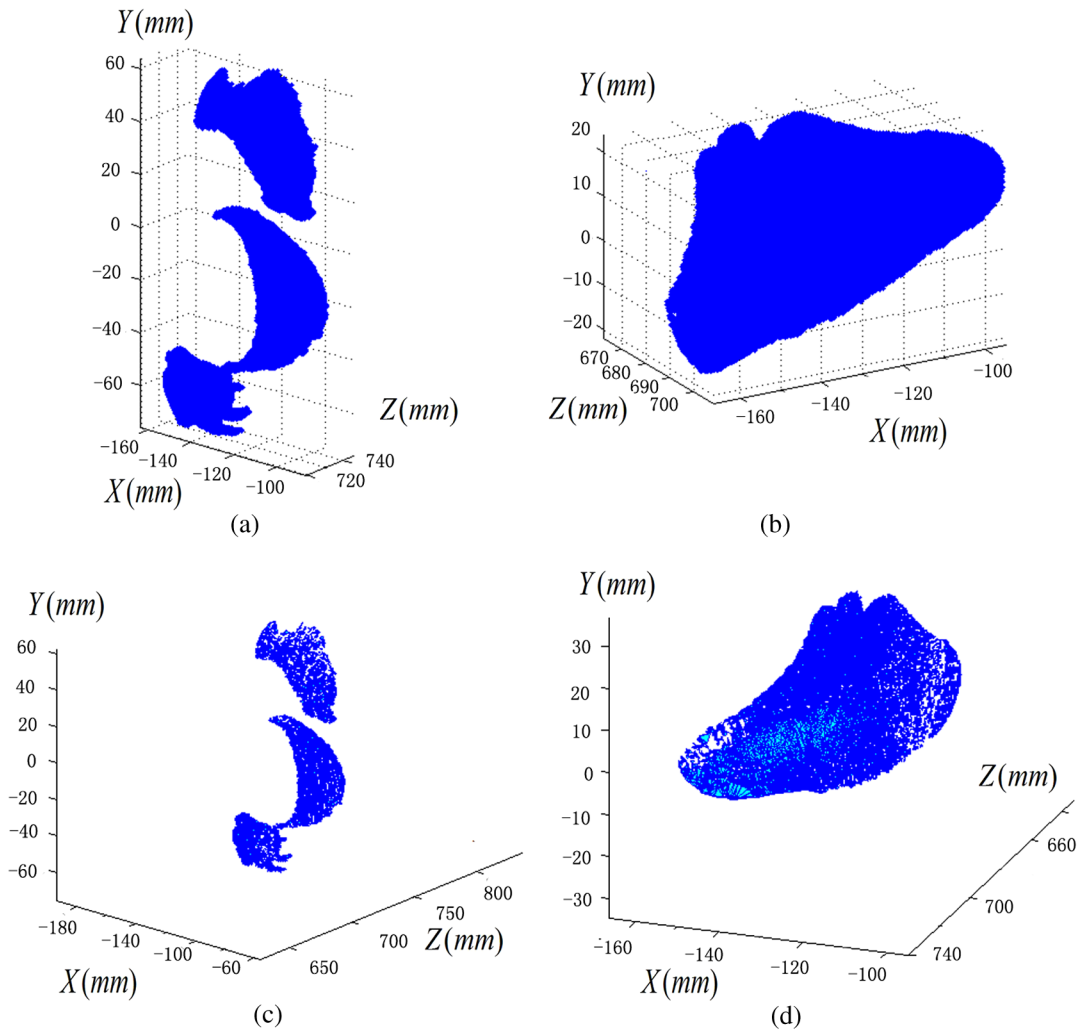
Fig. 5 Preprocessed point clouds in experiments (a) I and (b) II, and the triangle mesh model of lesions in experiments (c) I and (d) II.
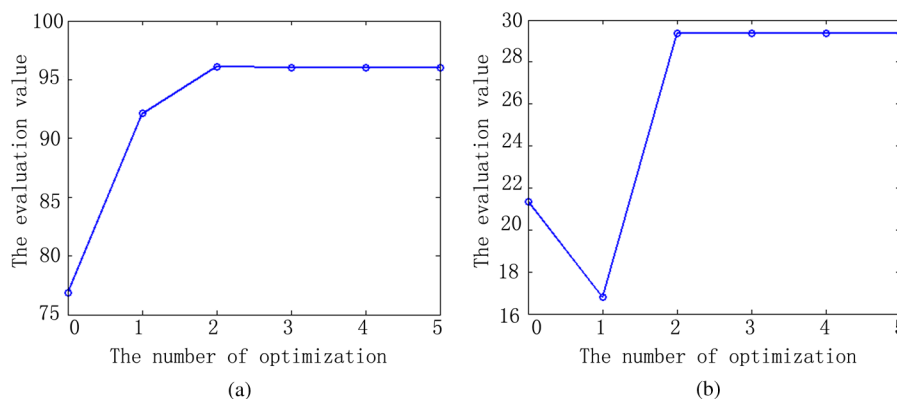
Fig. 6 Evaluation value in each optimization in experiments (a) I and (b) II.

3.4 Contrast Analysis

The irradiance received by a small patch is proportional to the cosine value of the irradiation angle when the optical power is constant. Given this relationship, this study used the area of the lesion patches within the same interval to estimate the distribution of the illumination area. The areas were compared before and after optimization to determine the effect of the proposed optimization method. The directions of the original and optimized irradiation are shown in Fig. 7. The sum of the area of the triangles within the same interval before and after optimization is shown in Fig. 8.

As indicated in Figs. 8(a) and 8(b), the majority of the irradiation angle of the lesions decreased and the area with higher
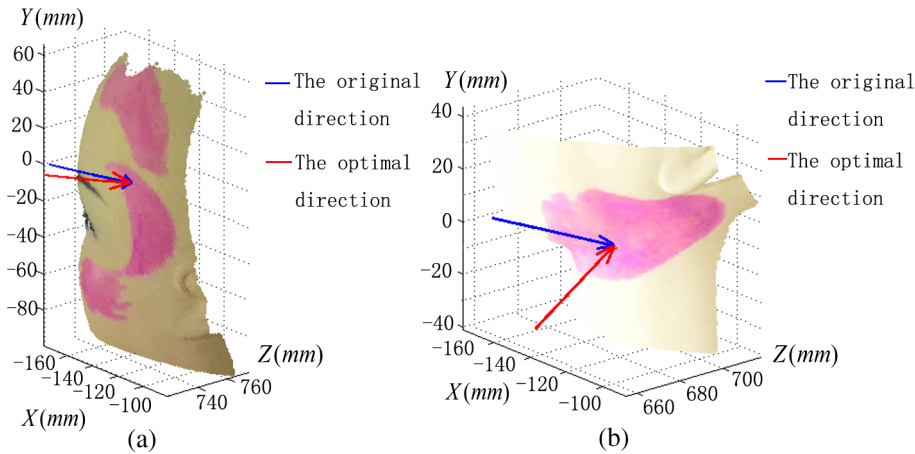
Fig. 7 Irradiation of the original and optimal directions in experiments (a) I and (b) II.
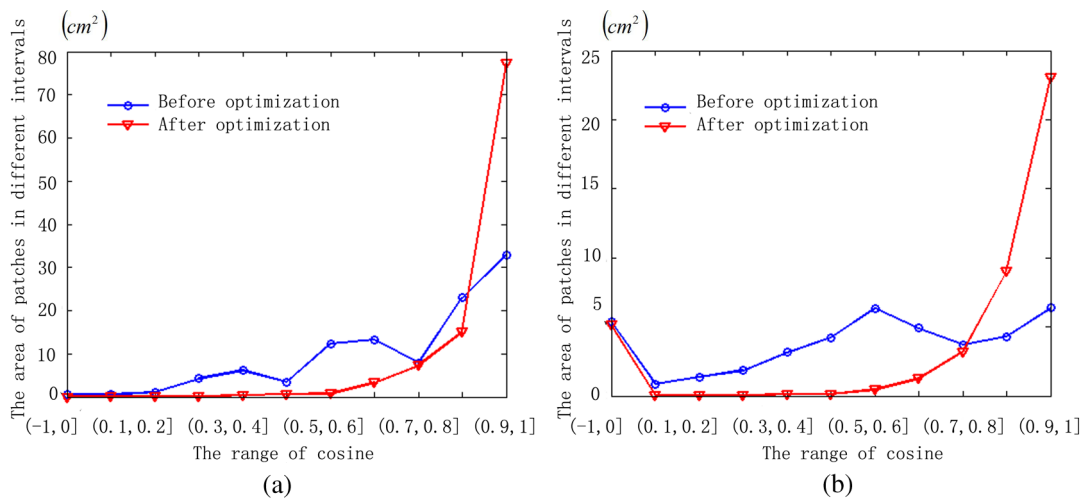
Fig. 8 Illumination area with different cosines before and after optimization in experiments (a) I and (b) II.

irradiance was improved, which revealed that the projector can effectively irradiate lesions in the optimal direction in each treatment session.

4 Discussion

4.1 Optical Parameters of the Human Skin

This study aimed to decrease the irradiation angle of lesions and improve light irradiance in each patch. Optical parameters (e.g., absorption coefficient, scattering coefficient, and photosensitizer absorption) of the human skin were not considered because of the limitations in the experimental conditions and clinical trials. The light absorbed by the photosensitizer was regarded as the effective light dose for PDT. This dose was unequal to the product of the optical density and irradiation time because of the varied complex light propagation in tissues and the optical coefficients of various tissues in different individuals.[33–35] The effective absorbed dose of lesions should be compensated when the individual optical properties of the tissue can be measured to improve the efficacy of irradiation. Thus, the optimization results can be evaluated in succeeding treatment sessions.

4.2 Light Source Requirement

The required irradiance was ∼100 mW/cm^2 for general PWS treatment. The power requirement of a light source can be estimated using Eq. (14) without considering the optical parameters of the lesion tissue.[24]

$$p = \frac{\mathrm{EHW}\beta^2}{\cos\theta(\cos\gamma)^4\eta}. \tag{14}$$

As indicated in Figs. 9(a) and 9(b), the required power of each patch was equal to the standard when the light source irradiated the lesions at the optimal direction in both experiments; as a result, the patches would receive the standard irradiance value. The 3-D irradiance map can be used by doctors to adjust the power of the light source and achieve uniform light distribution on lesions.

In the two experiments, the projector also irradiated the lesions by using different powers and revealed the illumination area with an irradiance satisfying the required dosage (Fig. 10). At a power of ∼8 W, the ratio of the effective area to the entire lesion for treatment could reach 98% in experiment I. At 5.7 W,
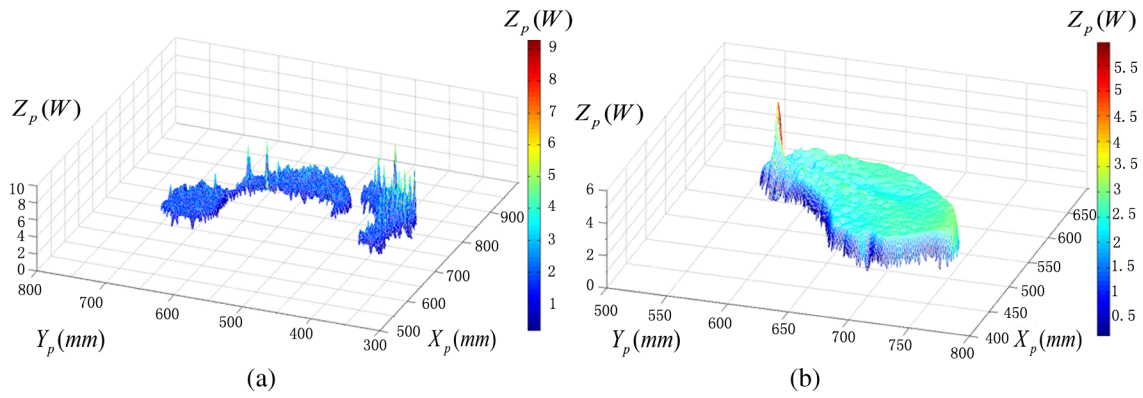
Fig. 9 Power required when lesions received the desired irradiance in experiments (a) I and (b) II.
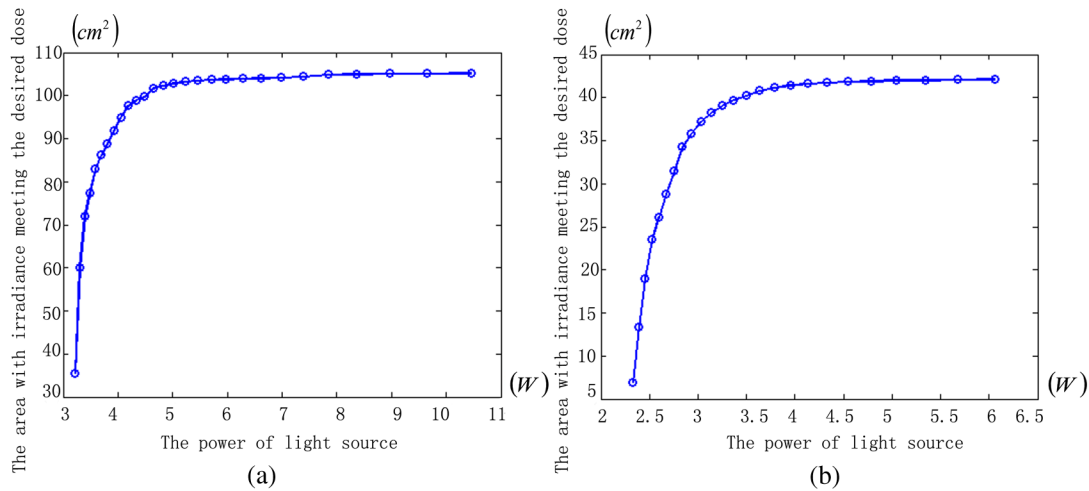
Fig. 10 Area with irradiance that satisfied the dosage requirement in experiments (a) I and (b) II.

the ratio could reach 99% in experiment II. Uniform light distribution can be achieved by modifying the gray value of the projection pixel that corresponds to the small patches on the lesions.

4.3 Severities of Lesions

PWS typically progresses from light pink to dark purple as the patient ages. These colors have been used as clinical indicators of PWS severity. The areas with different colors in the head model can be separately clustered via a superpixel method.[24] The severity of lesions in a patch can also be considered as another weight coefficient in the proposed optimization function. Severely affected regions can receive increased irradiance when the irradiation distribution is improved in the optimized direction within a specific power. After the expected light dosimetry of different lesions was established based on severities, and the required power was estimated using Eq. (14), a 3-D power map can guide doctors in adjusting the power of the light source to enable lesions with varying severities to receive optimum irradiance.

4.4 Factors Influencing Optimization

Control of irradiation direction is a complex optimization process affected by several factors. In the proposed optimization

Table 1 Execution performance of the optimization algorithm.

Experiment	Number of points in lesions	Number of triangle patches	Number of statistical intervals	Error of e $\Delta e = |e_{m+1} - e_m| \to \varepsilon$	Number of iterations	Time for proceeding
I	33,482	69,756	11	0.003%	5	13.8 s (the point cloud processing) + 5.73 s (optimization)
II	24,666	44,442	11	0.002%	5	7.5 s (the point cloud processing) + 4.86 s (optimization)

method, holes may exist in triangle mesh models because of defective data on the 3-D scanning point cloud. The defect area in the entire area of lesions was <1% in both experiments, so the holes minimally affected the optimization. Thus, the hole-fitting process was omitted to simplify the proposed method and reduce calculation requirements.

4.5 Feasibility Analysis of the Optimization Method

The point cloud processing was written in C++, and the optimization processing was written in MATLAB® on Microsoft Windows 7 32-bit platform. The execution performances of the two experiments are illustrated in Table 1. In terms of iterations and run-time, the proposed method can be applied in a treatment device to guide irradiation. A novel therapy device combined with the proposed digital illumination via a binocular treatment system incorporated with a robot arm could be an object of further research. The intelligent device that can perform individual therapy exhibits a significant potential in both research and clinical applications.

5 Conclusion

An optimization method to achieve the optimal irradiation direction in the PDT treatment is proposed in this research. The 3-D morphology and features of lesions provided objective and individualized information to set the weight coefficients, optimize the direction, and evaluate the effectiveness of the optimization. The proposed algorithm demonstrated the improvement and implementability with two experiments, which can be used to accurately set the irradiation direction and improve the efficiency of a single PDT treatment.

Acknowledgments

References

1. S. H. Barsky et al., "The nature and evolution of port-wine stains: a computer-assisted study," *J. Invest. Dermatol.* **74**(3), 154–157 (1980).
2. I. S. Carpintero et al., "Epithelial and mesenchymal hamartomatous changes in a mature port-wine stain: morphologic evidence for a multiple germ layer field defect," *J. Am. Acad. Dermatol.* **50**(4), 608–612 (2004).
3. W. Wang et al., "The pathological characteristics and clinical significances of maturational change of port wine stain," *Chin. J. Plast. Surg.* **26**(2), 103–106 (2010).
4. T. S. Lister, P. A. Wright, and P. H. Chappell, "Spectrophotometers for the clinical assessment of port wine stain skin lesions: a review," *Lasers Med. Sci.* **25**(3), 449 (2010).
5. T. S. Lister, P. A. Wright, and P. H. Chappell, "Simulating light transport through skin for color prediction of port wine stain lesions: a review," *J. Biomed. Opt.* **17**(11), 110901 (2012).
6. S. W. Lanigan and S. M. Taibjee, "Recent advances in laser treatment of port-wine stains," *Br. J. Dermatol.* **151**(3), 527–533 (2004).
7. C. J. Chang et al., "Comparing the effectiveness of 585-nm vs. 595-nm wavelength pulsed dye laser treatment of port wine stains in conjunction with cryogen spray cooling," *Lasers Surg. Med.* **31**(5), 352–358 (2002).
8. S. H. Woo et al., "Treatment of vascular skin lesions with the variable-pulse 595 nm pulsed dye laser," *Dermatol. Surg.* **32**(1), 41–48 (2006).
9. Z. F. Jasim and J. M. Handley, "Treatment of pulsed dye laser-resistant port wine stain birthmarks," *J. Am. Acad. Dermatol.* **57**(4), 677–682 (2007).
10. K. H. Yuan et al., "Photodynamic therapy in treatment of port wine stain birthmarks: recent progress," *Photodiagnosis Photodyn. Ther.* **6**(3-4), 189–194 (2009).
11. H. X. Qiu et al., "Twenty years of clinical experience with a new modality of vascular-targeted photodynamic therapy for port wine stains," *Dermatol. Surg.* **37**(11), 1603–1610 (2011).
12. Q. Xiao et al., "Photodynamic therapy of port-wine stains: long-term efficacy and complication in Chinese patients," *J. Dermatol.* **38**(12), 1146–1152 (2011).
13. W. X. Yu et al., "18 years long-term results of facial port-wine stain (PWS) after photodynamic therapy (PDT): a case report," *Photodiagnosis Photodyn. Ther.* **12**(1), 143–145 (2015).
14. K. H. Yuan et al., "Comparison of photodynamic therapy and pulsed dye laser in patients with port wine stain birthmarks: a retrospective analysis," *Photodiagnosis Photodyn. Ther.* **5**(1), 50–57 (2008).
15. K. Gao et al., "Side-by-side comparison of photodynamic therapy and pulsed-dye laser treatment of port-wine stain birthmarks," *Br. J. Dermatol.* **168**(5), 1040–1046 (2013).
16. B. Zhang et al., "Comparison of pulsed dye laser (PDL) and photodynamic therapy (PDT) for treatment of facial port-wine stain (PWS) birthmarks in pediatric patients," *Photodiagnosis Photodyn. Ther.* **11**(4), 491–497 (2014).
17. Y. Gu et al., "Clinical study of 1949 cases of port wine stains treated with vascular photodynamic therapy," *Ann. Dermatol. Venereol.* **134**(3), 241–244 (2007).
18. T. C. Zhu, J. C. Finlay, and S. M. Hahn, "Determination of the distribution of light, optical properties, drug concentration, and tissue oxygenation in-vivo in human prostate during motexafin lutetium-mediated photodynamic therapy," *J. Photochem. Photobiol. B* **79**(3), 231–241 (2005).
19. S. B. Brown, "The role of light in the treatment of non-melanoma skin cancer using methyl aminolevulinate," *J. Dermatol. Treat.* **14**(s3), 11–14 (2003).
20. Y. Wang et al., "New optional photodynamic therapy laser wavelength for infantile port wine stains: 457 nm," *J. Biomed. Opt.* **17**(6), 068003 (2012).
21. L. O. Svaasand et al., "Dosimetry model for photodynamic therapy with topically administered photosensitizers," *Lasers Med. Sci.* **11**(4), 261–265 (1996).
22. T. C. Zhu et al., "Real-time treatment feedback guidance of pleural PDT," *Proc. SPIE* **8568**, 85680O (2013).
23. X. T. Wang et al., "Development and clinical evaluation of medical robot assisted photodynamic therapy of port wine stains," *Int. J. Med. Robot.* **7**(1), 107–117 (2011).
24. X. M. Hu et al., "Three-dimensional illumination procedure for photodynamic therapy of dermatology," *J. Biomed. Opt.* **19**(9), 098003 (2014).
25. F. J. Zhang, X. M. Hu, and Q. S. Zhang, "The evaluation and planning of light dose in photodynamic therapy for port wine stains," *Proc. SPIE* **9268**, 926806 (2014).
26. D. Levin, "The approximation power of moving least-squares," *Math. Comput.* **67**(224), 1517–1531 (1998).
27. H. Zhang et al., "Consolidation of unorganized point clouds for surface reconstruction," *ACM Trans. Graph.* **28**(5), 176 (2009).
28. P. Breitkopf et al., "Moving least squares response surface approximation: formulation and metal forming applications," *Comput. Struct.* **83**(17), 1411–1428 (2005).
29. M. Alexa et al., "Computing and rendering point set surfaces," *IEEE Trans. Vis. Comput. Graph.* **9**(1), 3–15 (2003).
30. A. Nealen, "An as-short-as-possible introduction to the least squares, weighted least squares and moving least squares methods for scattered data approximation and interpolation," 2004, Tech. Rep., TU Darmstadt, http://www.nealen.net/projects/mls/asapmls.pdf (3 April 2015).
31. D. Levin, "Mesh-independent surface interpolation," in *Geometric Modeling for Scientific Visualization*, pp. 37–49, Springer, Berlin, Heidelberg (2004).
32. M. Pauly, "Point primitives for interactive modeling and processing of 3D geometry," PhD Thesis, Federal Institute of Technology (ETH) of Zurich (2003).
33. Y. Wang, F. G. Liu, and Y. Gu, "The effective absorbed light dose in photodynamic therapy and its measurement," *Acta Laser Biol. Sin.* **13**(2), 91–96 (2004).

34. S. L. Jacques, "How tissue optics affect dosimetry of photodynamic therapy," *J. Biomed. Opt.* **15**(5), 051608 (2010).
35. T. S. Lister, P. A. Wright, and P. H. Chappell, "Optical properties of human skin," *J. Biomed. Opt.* **17**(9), 090901 (2012).

Feng-juan Zhang received her BS degree in automation from Zhengzhou University in 2013 and is a candidate for the MS degree in biomedical engineering at Beijing Institute of Technology (BIT).

Xiao-ming Hu received his BS degree in physical electronics from BIT in 2001 and received his PhD in optical engineering from BIT in 2006. He has been working at the School of Life Science in BIT since then. His research interests include biomedical photonics, piezosurgery, and optical detection in microfluidics.

Ya Zhou received her PhD in optical engineering from BIT in 2000. After two years of postdoctoral research at School of Earth and Space Sciences, Peking University, she joined BIT as an associate professor in 2002. Her research interests include biometrics technology, medical image analysis, and computer vision.

Qin Li received her BS and MS degrees in physics from Capital Normal University in 1992 and 1995, respectively. She received her PhD degree in optical engineering from BIT in 1998.